Experimental Analysis of Diesel-Ignited Methane Dual-Fuel Low-Temperature Combustion in a Single-Cylinder Diesel Engine

Mostafa S. Raihan[1]; Edward S. Guerry[2]; Umang Dwivedi[3]; Kalyan Kumar Srinivasan[4]; and Sundar Rajan Krishnan[5]

Abstract: This paper focuses on the effect of diesel injection timing, intake boost pressure, and diesel injection pressure on diesel-methane dual-fuel combustion performed in a single-cylinder research engine. The engine was operated at a constant speed of 1,500 revolutions per minute (rpm) while percentage of methane energy substitution (PES) and load were maintained at 80% and 5.1 bar net indicated mean effective pressure (IMEP), respectively. The start of injection (SOI) of diesel was varied from 250 crank angle degrees (CAD) to 350 CAD while keeping the injection pressure at 500 bar and intake boost pressure at 1.5 bar. Advancing SOI from 330° to 300° reduced indicated specific NOx (ISNOx) emissions from 11.9 g/kW · h to less than 0.02 g/kW · h; further advancement of SOI did not yield any significant ISNOx reduction. Net indicated fuel conversion efficiency (IFCE) increases from 29.4% at 350 CAD SOI to 40.5% at 300 CAD SOI. Combustion efficiency trends are consistent with unburned hydrocarbon (HC) and carbon monoxide (CO) emission trends. Moreover, smoke emissions were lower than 0.1 filter smoke number (FSN) for all SOIs. A diesel injection pressure sweep from 200 to 1,300 bar at 300 CAD SOI showed that very low injection pressures lead to apparently more heterogeneous combustion and higher ISNOx, indicated specific CO (ISCO), and indicated specific HC (ISHC) emissions, whereas smoke, IFCE, and combustion efficiency remained unaffected. An injection pressure of approximately 500 bar appeared to be *optimal* for early SOIs. Finally, an intake boost pressure sweep from 1.1 to 1.8 bar at 300 CAD SOI and 500 bar injection pressure showed that ISNOx and smoke remained fairly low at all conditions (ISNOx < 0.15 g/kW · h; smoke < 0.1 FSN); however, increasing boost pressure resulted in an increase in both ISHC and ISCO emissions while combustion efficiency and IFCE were reduced. **DOI: 10.1061/(ASCE)EY.1943-7897.0000235.**

Author keywords: Low-temperature combustion; Dual-fuel combustion; Methane; NOx; Injection timing.

Introduction

Increasingly stringent exhaust emissions standards, the need for finding alternatives to liquid petroleum fuels, and the desire for higher fuel conversion efficiencies (FCEs) are key factors that have motivated research on advanced engine combustion strategies. Conventional diesel engines are constrained by tradeoffs between oxides of nitrogen (NOx) and particulate matter (PM) emissions. Current U.S. Environmental Protection Agency (USEPA) regulations for brake-specific PM and NOx emissions from heavy-duty diesel engines are 0.013 and 0.268 g/kW · h, respectively (DieselNet 2014). Simultaneous reduction of NOx and PM emissions without sacrificing fuel conversion efficiency (FCE) is an inherent challenge with conventional diesel combustion. In contrast, several low-temperature combustion (LTC) concepts that promise low NOx and PM have been investigated over the last decade (Dec 2009; Musculus et al. 2013). Alternatives to fossil-based fuels, including natural gas (Beck et al. 1997; Wong et al. 2000), propane (Goldsworthy 2012; Polk et al. 2014a), and biofuels from various sources (Agarwal 2007; Contino et al. 2013; Giakoumis et al. 2013; Lee et al. 2013; Sayin 2010) also have been considered. Although various biodiesel blends can be used in existing diesel engines without any hardware modifications, the NOx emissions are normally higher with biodiesel operation (Giakoumis et al. 2013).

In conventional diesel combustion, as described by Dec (1997), PM formation occurs in rich premixed combustion regions whereas NOx forms in the hot, near-stoichiometric mixtures of the diffusion flame surrounding the jet. Because NOx formation rates increase exponentially with temperature, in-cylinder NOx control strategies typically use exhaust gas recirculation (EGR) to reduce local temperatures (Zheng et al. 2004). However, excessive EGR used with some LTC strategies can lead to poor combustion efficiencies (Huestis et al. 2007) because of the presence of high unburned hydrocarbon (HC) and carbon monoxide (CO) in the combustion products.

To address the challenge of simultaneous NOx and PM reduction in diesel engines, dual-fuel combustion has been investigated with a variety of alternative fuels, including natural gas, propane, and biogas (Gibson et al. 2011; Karim 2003; Krishnan et al. 2004; Kusaka et al. 2000; McTaggart-Cowan et al. 2006;

[1]Graduate Student, Dept. of Mechanical Engineering, Mississippi State Univ., 210 Carpenter Building, Mississippi State, MS 39762. E-mail: mr1158@msstate.edu

[2]Graduate Student, Dept. of Mechanical Engineering, Mississippi State Univ., 210 Carpenter Building, Mississippi State, MS 39762. E-mail: esguerry@gmail.com

[3]Graduate Student, Dept. of Mechanical Engineering, Mississippi State Univ., 210 Carpenter Building, Mississippi State, MS 39762. E-mail: umang_dwivedi@yahoo.com

[4]Associate Professor, Dept. of Mechanical Engineering, Mississippi State Univ., 210 Carpenter Building, Mississippi State, MS 39762. E-mail: srinivasan@me.msstate.edu

[5]Associate Professor, Dept. of Mechanical Engineering, Mississippi State Univ., 210 Carpenter Building, Mississippi State, MS 39762 (corresponding author). E-mail: krishnan@me.msstate.edu

Note. This manuscript was submitted on May 25, 2014; approved on August 1, 2014; published online on September 5, 2014. Discussion period open until February 5, 2015; separate discussions must be submitted for individual papers. This paper is part of the ***Journal of Energy Engineering***, © ASCE, ISSN 0733-9402/C4014007(13)/$25.00.

Papagiannakis and Hountalas 2004; Polk et al. 2013, 2014a, b; Tira et al. 2014). Dual-fuel combustion utilizes an easily ignitable, high-cetane, pilot fuel to ignite an autoignition-resistant, low-cetane, primary fuel, which is typically premixed along with air in the intake manifold and introduced into the cylinder during the intake stroke. Several high-cetane pilot fuels such as diesel (Badr et al. 1999; Krishnan et al. 2002; Selim 2004; Srinivasan et al. 2006a), biodiesel (Bedoya et al. 2009; Debnath et al. 2013; Ryu 2013a, Shoemaker et al. 2012), and dimethyl ether (Chen et al. 2009; Yao et al. 2006) have been considered. Of the various primary fuels discussed, natural gas, which has methane as the major constituent, is a popular choice for many dual-fueling applications. The relative percentage of natural gas and diesel, the injection timing of diesel, and the availability of air within the cylinder play major roles in the dual-fuel combustion process (Liu and Karim 1995; Karim 2003; Papagiannakis and Hountalas 2003). Karim (2003) divided conventional diesel-ignited methane dual-fuel combustion into three distinct stages. After an ignition delay period, the diesel fuel releases energy and initiates the combustion process, which in turn ignites the surrounding methane-air mixture. Lastly, combustion proceeds by flame propagation through the remainder of the lean methane-air mixture. Although dual-fuel engines exhibit some advantages over conventional diesel engines such as higher fuel conversion efficiencies and lower emissions under certain engine operating conditions, they tend to knock at high loads (Liu and Karim 1995) and produce higher HC from crevices and bulk quenching and CO emissions partial fuel oxidation at low loads (Srinivasan 2006b; Papagiannakis et al. 2010).

To further reduce NOx and PM emissions to meet current USEPA regulations, several dual-fuel LTC strategies have been pursued. For example, the advanced low pilot ignited natural gas (ALPING) dual-fuel LTC concept was demonstrated (Krishnan et al. 2004; Qi et al. 2007; Srinivasan et al. 2006a, b, 2007). In ALPING dual-fuel LTC, approximately 97–98% of the total fuel energy is supplied by natural gas, whereas diesel is used only as an ignition source using a dedicated micropilot injection system. The ALPING concept yielded good FCEs and extremely low engine-out NOx emissions (<0.2 g/kW · h); however, these benefits were accompanied by excessive HC and CO emissions (Krishnan et al. 2004). Subsequent experiments on ALPING dual-fuel LTC used hot EGR and intake charge heating to achieve up to 70% HC reductions along with low NOx and high FCE benefits at low loads (Qi et al. 2007). Similarly, diesel-ignited propane dual-fuel LTC was recently demonstrated with very similar NOx emissions benefits on a multicylinder heavy-duty diesel engine (Polk et al. 2014a). Another dual-fuel LTC strategy that involves diesel ignition of gasoline-air mixtures is reactivity controlled compression ignition (RCCI) (Hanson et al. 2010; Kokjohn et al. 2011; Splitter et al. 2011). Diesel-propane LTC, ALPING dual-fuel LTC, and RCCI are all based on the idea that in-cylinder stratification of fuel reactivity between the low-cetane primary fuel and the high-cetane diesel pilot can be exploited to control the partially premixed combustion process.

Several past studies have focused on the characterization of diesel-ignited natural gas dual-fuel combustion (Daisho et al. 1995; Kusaka et al. 2000; Selim 2004; Papagiannakis et al. 2010). In addition, the effects of critical engine parameters such as pilot fuel quantity (Abd Alla et al. 2000; Krishnan et al. 2004; Papagiannakis and Hountalas 2003; Papagiannakis et al. 2007), pilot injection timing (Abd Alla et al. 2002; Krishnan et al. 2004; Ryu 2013a; Sayin et al. 2008; Sayin and Canakci 2009), pilot injection pressure (Carlucci et al. 2008; Jindal et al. 2010; Ryu 2013b), and boost pressure (Krishnan et al. 2002; Singh et al. 2004) on dual-fuel combustion have been investigated. For example, Carlucci et al. (2008) studied the effects of injection pressure (600–1,000 bar) and found that NOx emissions decreased with increasing injection pressure whereas CO emissions showed the opposite trend. These results are also supported by McTaggart-Cowan et al. (2004) for high load conditions. However, in both of these studies, the pilot injection timing was fixed close to top dead center (TDC) and the injection pressure variation was relatively narrow. Abd Alla et al. (2002) reported improvement in FCE and reduction in HC and CO emissions with the advancement of pilot injection timing and a slight increase in NOx emissions. However, again, the scope of this study was also limited to injection timing variations between 325 CAD and 330 CAD. Polk et al. (2013) and Gibson et al. (2011) presented data of diesel-ignited methane dual-fuel combustion on a turbocharged multicylinder light-duty engine but these data were limited by the use of the stock engine controller. Papagiannakis et al. (2007) suggested that a proper combination of injection timing and injection quantity might lead to lower CO emissions and higher FCEs.

Objectives of the Present Work

The primary objective of the present work is to investigate the performance and emission characteristics of diesel-ignited methane dual-fuel combustion in a single-cylinder research engine (SCRE) at a constant engine load of 5.1 bar net indicated mean effective pressure (IMEP) and at a constant engine speed of 1,500 revolutions per minute (rpm). Engine control parameters such as injection timing, injection pressure, and intake boost pressure are systematically varied, while keeping all other parameters constant, to quantify the effect of each parameter on the performance and emissions. First, an injection timing study is performed between 250 CAD and 350 CAD at 5.1 bar IMEP, 1,500 rpm, and fixed injection pressure and intake boost pressure. Then, an optimal SOI is chosen based on the performance and emissions results, which is subsequently used for injection pressure and intake boost pressure studies from 200 to 1,300 bar and 1.1 to 1.8 bar, respectively.

Experimental Setup

Fig. 1 shows a schematic of the experimental setup used in the present study. A four-stroke, compression ignition SCRE was used to conduct all experiments. Relevant engine specifications are given in Table 1. The engine was coupled to a 250-HP AC regenerative dynamometer, which was controlled by an Inter-Lock V controller that also provided torque and speed measurements. Intake, exhaust, coolant, and oil temperatures were measured using Omega Type-K thermocouples. Gaseous and exhaust emissions were measured downstream of the exhaust manifold using an emissions sampling trolley and an integrated emissions bench (EGAS 2M) manufactured by Altech Environment S.A. The EGAS 2M bench measured total hydrocarbon emissions (THC) with a heated flame ionization detector, NOx emissions with a chemiluminescence detector, carbon dioxide and carbon monoxide emissions with a nondispersive infrared analyzer, and oxygen with a paramagnetic detector. Smoke was measured in filter smoke number (FSN) units using an AVL 415S (AVL, Graz, Austria) variable sampling smoke meter.

Pilot diesel flow rate and methane flow rate were measured with Emerson Micro Motion coriolis mass flow meters. A Bosch CP3 (Bosch, Stuttgart, Germany) common-rail fuel injection pump and injector were used to inject diesel. Diesel injection parameters were controlled by a Drivven stand-alone diesel injection (SADI) driver coupled with CALVIEW software (National Instruments, Austin, Texas). A HANBAY needle valve (Model MCM-050AB)

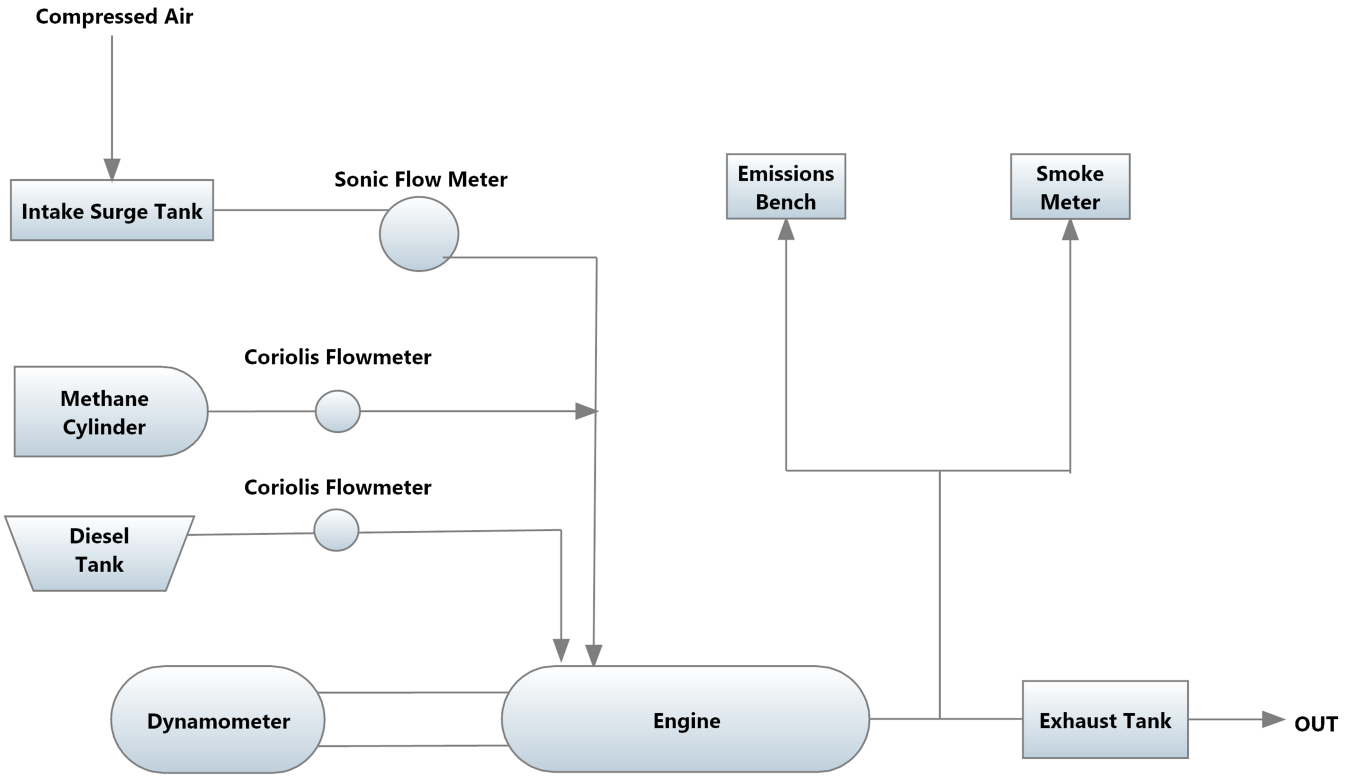

Fig. 1. Schematic of the experimental setup

Table 1. Single-Cylinder Research Engine (SCRE) Specifications

Parameter	Specification
Bore × stroke (mm × mm)	128 × 142
Connecting rod length (mm)	228
Displaced volume (cc)	1,827
Compression ratio	17.1:1
Combustion chamber geometry	Mexican hat
Valve timings	IVO—32 CAD, IVC—198 CAD EVO—532 CAD, EVC—14 CAD
Diesel fuel injection system	Bosch CP3 common-rail
Injector nozzle hole diameter (mm)	0.197
Number of nozzle holes	8
Methane fuelling	Fumigation into intake manifold
Maximum speed (rpm)	1,900

Note: EVC = exhaust valve closing; EVO = exhaust valve opening; IVC = intake valve closing; IVO = intake valve opening.

(Hanbay, Montreal, Canada) was used to control the flow rate of methane, which was fumigated in the intake manifold.

The in-cylinder pressure was measured using a Kistler model 6052C pressure sensor and a Kistler 5010B type charge amplifier (Kistler, Winterthur, Switzerland). The diesel injector was instrumented with a Wolff Hall effect sensor (Wolff Controls Corporation, Winter Haven, Florida) to obtain the needle lift data. Both sensors were phased with respect to crank angle using a BEI incremental shaft encoder (BEI Sensors, Goleta, California) with a resolution of 0.1 crank angle degree (CAD), which was coupled to the engine crankshaft. Cylinder pressure and needle lift data were recorded and averaged over 100 consecutive cycles, and an intake manifold pressure sensor was used to peg the cylinder pressure data at bottom dead center (BDC). It is well known from the literature that dual-fuel combustion, utilizing diesel as the ignition source and any low cetane fuel as the primary fuel, tends to exhibit significant cyclic variations depending on the concentration of primary fuel and engine operating parameters (Rakopoulos et al. 2013; Selim 2005). In the present study, cyclic combustion variations in 100 consecutive cycles are quantified as the coefficient of variation (COV) of indicated mean effective pressure (IMEP), which is the ratio of the standard deviation in IMEP to the arithmetic mean of the IMEP expressed as a percentage. A more detailed study of cyclic combustion variations may require data acquired over many more cycles, and therefore, is outside the scope of the present work. To simulate intake boosting, an Atlas Copco air compressor (Model GA75) (Atlas Copco Compressors, Rock Hill, South Carolina) coupled with a heatless desiccant dryer (Model CD 250) were used. Air flow rate was measured using a FlowMaxx sonic orifice (Model SN16-SA-235) (Flow Maxx Engineering, Fort Worth, Texas). To ensure choked flow across the sonic orifice at all engine operating conditions, the pressure ratio across the orifice (inlet to outlet) was always maintained above a critical value of 1.2. Subsequently, air mass flow rate was directly determined from the sonic orifice calibration curve by measuring the pressure and temperature upstream of the sonic orifice. Temperature of the intake air was maintained at around 30°C. All of the steady-state data were recorded and averaged over 60 s. The measured experimental parameters and their accuracies are summarized in Table 2.

Definitions

To clarify the various terms used in this paper, relevant parameters such as equivalence ratio (Φ), percent energy substitution (PES), ignition delay (ID), combustion efficiency (ηc), indicated fuel conversion efficiency (IFCE), apparent heat release rate (AHRR), and the ratio of specific heats (γ) are defined

$$\text{PES} = \frac{\dot{m}_g \text{LHV}_g}{\dot{m}_d \text{LHV}_d + \dot{m}_g \text{LHV}_g} \quad (1)$$

Table 2. Accuracies of Various Experimental Measurements

Measured parameters	Unit	Accuracy
Engine speed	rpm	±1 rpm of reading
Engine torque	Nm	±0.06% of reading
Cylinder pressure	bar	±0.005 of reading
Diesel flow rate	kg/h	±0.05% of reading
Methane flow rate	kg/h	±0.35% of reading
Air flow rate	kg/h	±0.1% of reading
Temperatures	°C	±0.75% of reading
Pressures (intake, exhaust, coolant, and lubrication oil)	psig	±0.25% of reading
Smoke number	FSN	±0.001 of reading
THC emissions	ppm	<0.5% of full scale
NOx emissions	ppm	<1% of full scale
CO	%	<1% of full scale
CO_2	%	<1% of full scale
O_2	%	<1% of full scale

$$\Phi = \frac{\left(\frac{A}{F}\right)_{\text{st-tot}}}{\left(\frac{\dot{m}_a}{\dot{m}_d+\dot{m}_g}\right)} \tag{2}$$

$$\text{ID} = \text{CA5} - \text{SOI} \tag{3}$$

$$\eta_c = 1 - \frac{\sum x_f \text{LHV}_f}{\frac{\dot{m}_f}{\dot{m}_a+\dot{m}_f}} \tag{4}$$

$$\text{IFCE} = \frac{\text{IP}}{\dot{m}_d \text{LHV}_d + \dot{m}_g \text{LHV}_g} \tag{5}$$

$$\text{AHRR}(\theta) = \frac{\gamma}{\gamma-1} P \frac{dV}{d\theta} + \frac{1}{\gamma-1} V \frac{dP}{d\theta} \tag{6}$$

$$\gamma = 1.338 - 6 \times 10^{-5} T + 1 \times 10^{-8} T^2 \tag{7}$$

In Eqs. (1) and (2), $\dot{m}$ refers to the mass flow rates of diesel (subscript d), methane (subscript g), and air (subscript a), and LHV refers to the corresponding lower heating values of the fuels. Stoichiometric air-fuel ratio $(A/F)_{\text{st-tot}}$ is defined as the stoichiometric air required for complete oxidation of both diesel and methane into CO_2 and H_2O. Therefore, $(A/F)_{\text{st-tot}}$ depends on the PES of methane. The start of combustion is defined as Crank angle corresponding to 5% of cumulative heat release (CA5) or the crank angle at which 5% of cumulative heat release occurs. In Eq. (4), combustion efficiency (η_c) is normally calculated using the mass fractions (x_f) of CO, H_2, HC, and PM using their respective LHVs. Because the composition of HC in the exhaust, and thus its LHV, are not known, Heywood (1988) recommends using the LHV of the fuel as they are expected to of comparable magnitude. However, for this study, because two fuels were used, the combined mass-fraction-weighted LHV of diesel and methane is used to represent the LHV of HC. Also, because gravimetric PM was not measured in the present experiments, it was not considered in the combustion efficiency calculations. The net IFCE was calculated as shown in Eq. (5) using the net indicated power estimated from the measured cylinder pressure data and the measured fuel flow rates and their respective LHVs. The net apparent heat release rate (AHRR) presented in this paper was derived from measured in-cylinder pressure data using Eq. (6). The instantaneous volume (V) was calculated from the engine geometry and derivatives of pressure and volume ($dP/d\theta$ and $dV/d\theta$) were calculated numerically using a four-point central difference formula. The specific heat ratio (γ) required in Eq. (6) was evaluated as a function of mass averaged temperature (T) using Eq. (7) (Brunt et al. 1998). In this regard, it may be observed that there are more sophisticated models for deriving gross and net heat release rates from experimental cylinder pressure data that may account for heat transfer to cylinder walls and different compositions for burned and unburned gases (Rakopoulos et al. 2010; Krishnan et al. 2002). However, because the objective of the present work was to compare heat release trends in dual-fuel LTC rather than the precise determination of gross heat release rates, the simpler net AHRR approach described previously was adopted. Combustion phasing is defined as the crank angle at which 50% of the cumulative heat release occurs and denoted as crank angle corresponding to 50% of cumulative heat release (CA50). Also, crank angle duration between 10 and 90% cumulative heat release (CA10-90), which is defined as the difference between the crank angle at which 10% of cumulative heat release occurs and the crank angle at which 90% of cumulative heat release occurs, gives an estimation of overall combustion duration.

Results and Discussions

Diesel Injection Timing (SOI) Effects

For the SOI experiments, the engine was operated at 5.1 bar IMEP, 1,500 rpm, and 80 PES, whereas SOI was varied from 350 to 250 CAD. Diesel injection pressure and intake boost pressure were kept constant at 500 and 1.5 bar, respectively, and no EGR was used.

Figs. 2 and 3 present cylinder pressure profiles and AHRR curves at different SOIs. As SOI is advanced from 350 CAD to 250 CAD, the shapes of the AHRR curves and combustion characteristics change significantly. For convenience and better understanding of the results, cylinder pressure profiles and AHRR are plotted separately for early and late SOIs. As SOI is advanced from 350 CAD to 330 CAD, peak AHRR values increase. The AHRR curves also exhibit two distinct stages and no significant low-temperature heat release (LTHR) peak because of relatively high in-cylinder temperatures for late SOIs. Another feature to be noted is that there was very little or no separation between the end of injection (EOI) and the start of combustion (SOC) of the main combustion event for these SOIs. For example, for the SOI of 330 CAD, the difference between SOC and EOI is approximately 1 CAD as fuel injection finishes at 340 CAD and combustion starts at around 341 CAD. For the other two SOIs of 350 CAD and 340 CAD, combustion starts even before EOI.

As SOI is advanced further in the compression stroke, the separation between EOI and SOC is increased. For the SOI of 320 CAD, the separation between SOC and EOI is approximately 7 CAD, whereas for the SOI of the separation, it increases to approximately 15 CAD. As SOI is advanced to 250 CAD, the peak magnitude of AHRR decreases and the peak AHRR is phased almost at or beyond TDC. Also as SOI is advanced from 310 CAD to 250 CAD, the LTHR vanishes and a smooth AHRR curve that may represent *well mixed* diesel-ignited methane LTC is observed.

Fig. 4 shows trends for maximum pressure rise rate (MPRR), ID, and COV of IMEP versus SOI. It is evident from Fig. 4 that while ID increases when SOI is advanced beyond 330 CAD, MPRR peaks near 330 CAD and is reduced for earlier and later SOIs. Also, as SOI is advanced, COV of IMEP decreases at first from 4.0% at 350 CAD to 1.6% at 320 CAD and increased with further SOI advancement. The highest COV of IMEP of 9% occurred at the SOI of 250 CAD, indicating that combustion

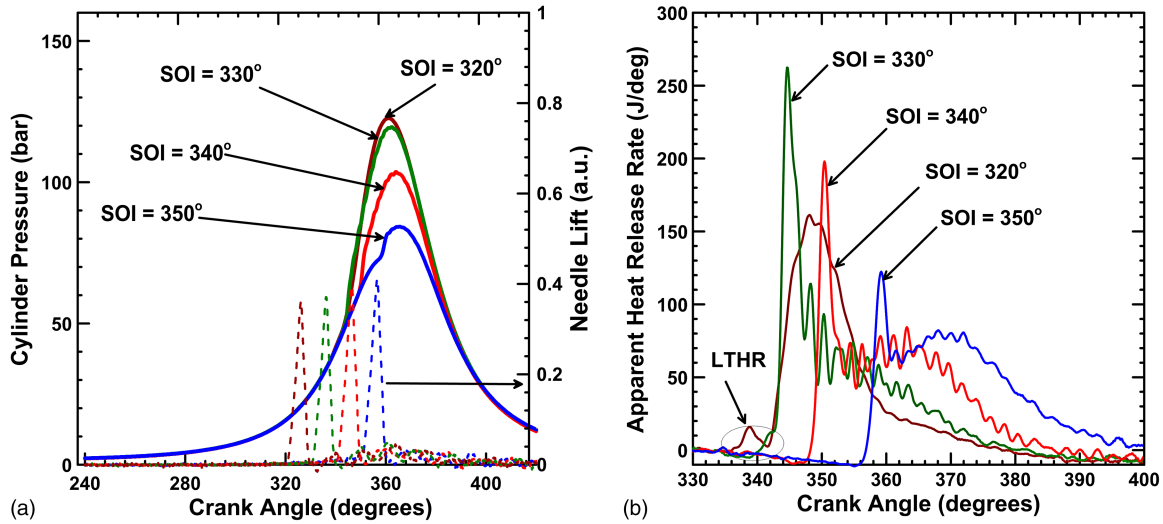

Fig. 2. (a) Cylinder pressure and needle lift profiles for late SOIs at 5.1 bar IMEP, 80 PES, $N = 1{,}500$ rpm, Pin = 1.5 bar; (b) AHRR schedules for late SOIs at 5.1 bar IMEP, 80 PES, $N = 1{,}500$ rpm, Pin = 1.5 bar

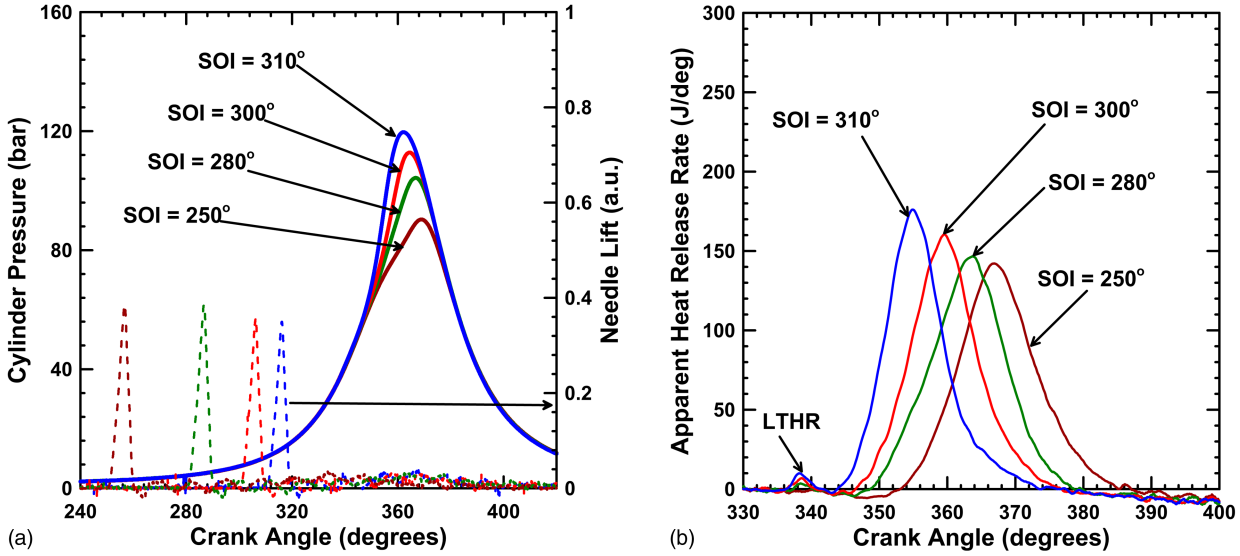

Fig. 3. (a) Cylinder pressure and needle lift profiles for early SOIs at 5.1 bar IMEP, 80 PES, $N = 1{,}500$ rpm, Pin = 1.5 bar; (b) AHRR schedules for early SOIs at 5.1 bar IMEP, 80 PES, $N = 1{,}500$ rpm, Pin = 1.5 bar

becomes increasingly unstable because of increasing homogeneity (and presumably weaker ignition centers) as SOI is advanced. Fig. 5 shows that the combustion duration (CA10-90) decreases from approximately 23 CAD to approximately 12 CAD between SOIs of 350 CAD and 310 CAD and increases slightly for more advanced SOIs. Also, CA50 shifts from after TDC to before TDC as SOI is advanced from 350 CAD to 320 CAD and again swings back to after TDC upon further SOI advancement. These trends can be traced to the transition from two-stage AHRR curves at late SOIs to smooth single-stage AHRR curves that are progressively retarded with respect to TDC as SOI is advanced.

Fig. 6 shows ISNOx and smoke trends for different SOIs. As SOI is advanced from 350 CAD to 330 CAD, ISNOx sharply increases from approximately 2.4 g/kW · h to approximately 11.9 g/kW · h. However, on further SOI advancement to 310 CAD and beyond, ISNOx decreases significantly from 11.9 g/kW · h to near-zero levels (0.015 g/kW · h). Near-zero ISNOx levels for sufficiently early SOIs are the cumulative effect of increased residence times, separation of EOI and SOC, and more complete fuel-air mixing leading to lean homogeneous fuel-air mixtures, all of which lead to low local temperatures. The smoke emissions, which were less than 0.1 FSN for the entire SOI sweep, remain low because of the relatively high PES of methane (80%) coupled with the fact that the combustion process occurs in predominantly lean regions within the cylinder under these operating conditions. Simultaneous reductions in ISNOx and smoke emissions indicate that dual-fuel LTC has been attained for SOIs at and beyond 310 CAD.

Fig. 7 shows the effects of SOIs on IFCE and combustion efficiencies at 5.1 bar IMEP and 80 PES. Combustion efficiency increases with SOI advancement from 340 CAD to 290 CAD and reaches the highest value of 86.1%, indicating that the HC and CO emissions are near the lowest levels at this SOI (Fig. 8).

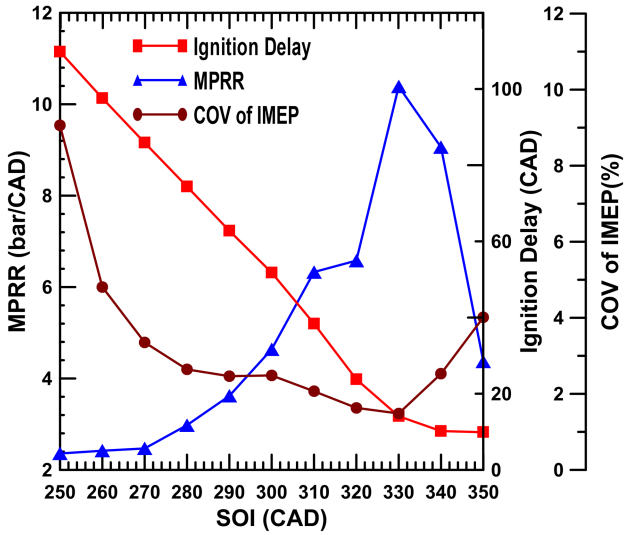

Fig. 4. MPRR, ignition delay, and coefficient of variation of IMEP versus SOI at 5.1 bar IMEP, 80 PES, N = 1,500 rpm, Pin=1.5 bar

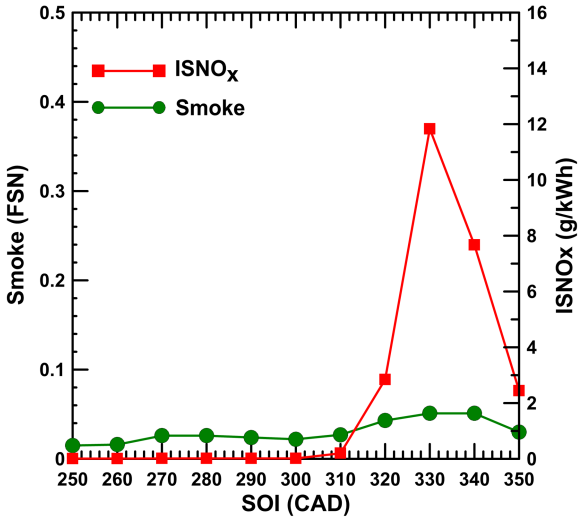

Fig. 6. ISNOx and smoke emissions versus SOI at 5.1 bar IMEP, 80 PES, N = 1,500 rpm, Pin = 1.5 bar

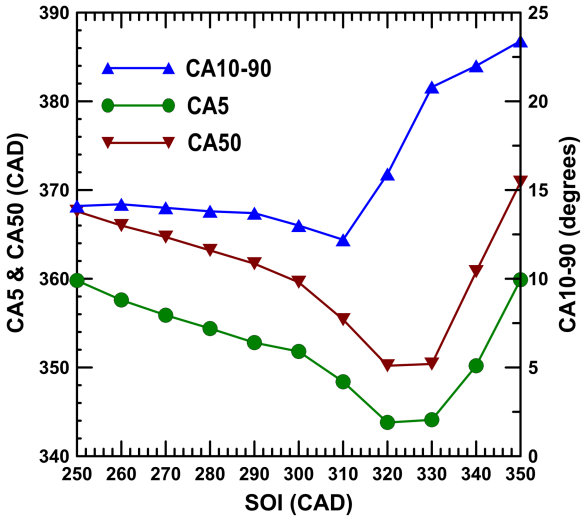

Fig. 5. CA5, CA50, and CA10-90 versus SOI at 5.1 bar IMEP, 80 PES, N = 1,500 rpm, Pin = 1.5 bar

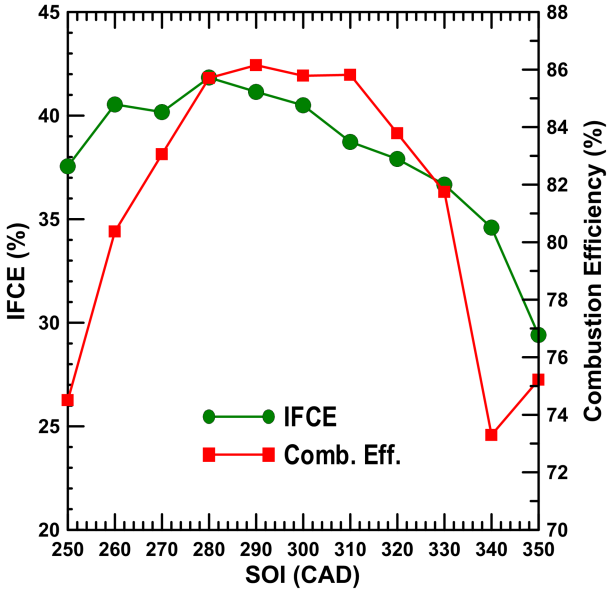

Fig. 7. Combustion and indicated fuel conversion efficiencies versus SOI at 5.1 bar IMEP, 80 PES, N = 1,500 rpm, Pin = 1.5 bar

Also, IFCE increases from 29.4 to 40.5% as SOI is advanced from 350 CAD to 300 CAD. This increase in IFCE can be related to the AHRR, CA50, and CA10-90 trends as well as the increased combustion efficiencies at the advanced SOIs. For further SOI advancement from 280 CAD to 250 CAD, both combustion efficiency and IFCE decrease because of retarded CA5 and CA50 and sharply increasing HC and CO emissions.

Fig. 8 shows the ISCO and ISHC emissions trends between SOIs of 350 CAD and 250 CAD. The ISCO decreases from approximately 16.2 g/kW · h at 350 CAD SOI to 7.3 g/kW · h at 310 CAD SOI and then increases to 25 g/kW · h at the most advanced SOI of 250 CAD. A decrease in ISHC is also observed from 49.6 to 17.1 g/kW · h when SOI is advanced from 350 CAD to 280 CAD and then increases to 31.5 g/kW · h at 250 CAD SOI.

The manifestation of very high ISHC at the SOIs of 350 CAD and 340 CAD can be explained by the CA50 and CA10-90 trends. At the outset, it must be recognized that combustion chamber crevices are likely significant sources of HC in the present scenario where methane is fumigated into the intake manifold. In contrast, bulk quenching because of mixing of hotter post-combustion gases with cooler surroundings may also lead to CO and HC formation. At the retarded SOIs of 350–340 CAD and the very advanced SOIs of 260 CAD–250 CAD, the CA50 occurs at nearly 10 CAD after TDC, and consequently, the bulk of the combustion process occurs during the expansion stroke. Oxidation of CO and HC are significantly influenced by the in-cylinder temperatures and the residence times of hot postcombustion gases in the combustion chamber. Because the bulk of the combustion occurs after TDC, the peak in-cylinder temperatures for these retarded SOIs are relatively lower, thereby leading to high engine-out ISHC emissions under these conditions.

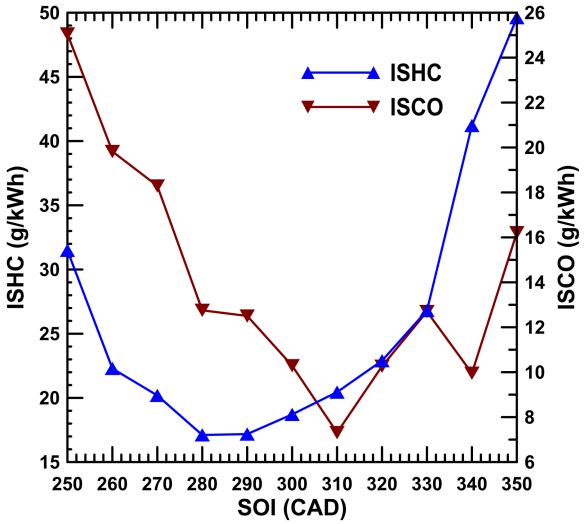

Fig. 8. ISHC and ISCO emissions versus SOI at 5.1 bar IMEP, 80 PES, $N = 1{,}500$ rpm, Pin = 1.5 bar

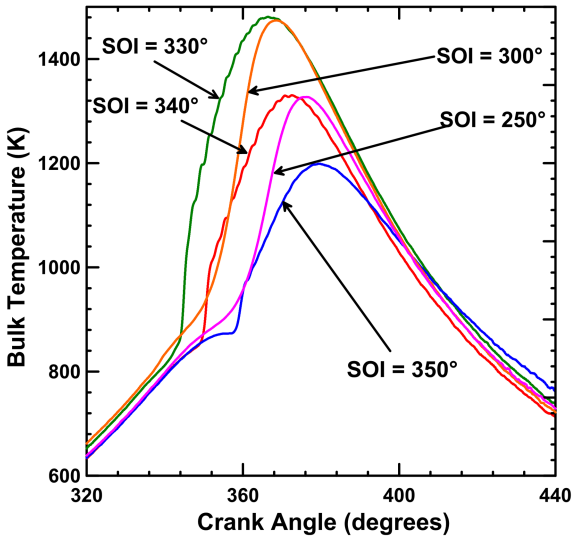

Fig. 9. Bulk gas temperature schedules for various SOIs at 5.1 bar IMEP, 80 PES, $N = 1{,}500$ rpm, Pin = 1.5 bar

The CO emissions attain the lowest levels for SOIs between 320 CAD and 300 CAD. This is because the CA50 is phased closer to TDC; so the mass-averaged bulk gas temperatures are higher and support CO oxidation during the expansion process as shown in Fig. 9. On further advancement of SOIs from 300 CAD to 280 CAD, it is possible that competition between HC and CO oxidation reactions resulted in high CO emissions. Because HC oxidation rates are much faster than CO, HC is oxidized and CO increases. To support this theory, mass-averaged bulk gas temperatures, determined using the ideal gas equation of state along with measured cylinder pressure and known cylinder volume histories, for different SOIs are plotted in Fig. 9. It is evident that for very advanced or very retarded SOIs, the overall bulk gas temperatures are lower than those of intermediate SOIs. This reduction in peak bulk gas temperature likely reduced the availability of OH radicals in the lean premixed diesel-methane-air mixture surrounding the diesel jet. Also, as CO oxidation occurs later in the combustion process after the oxidation of the original fuel molecules, it is possible that HC is oxidized early in the combustion process but late-cycle CO oxidation is perhaps limited by lower bulk gas temperatures and less time available for the CO oxidation reactions to be completed.

Injection Pressure Effects

For the injection pressure sweep, the engine was operated at 5.1 bar IMEP, 1,500 rpm, 80 PES, 300 CAD SOI, and an intake boost pressure of 1.5 bar while the injection pressure was varied from 200 to 1,300 bar.

Figs. 10(a and b) present cylinder pressure and AHRR profiles for injection pressures ranging from 200 to 1,300 bar. As injection pressure increases from 200 to 1,300 bar, the cylinder pressure profile shifts away from TDC. From the needle lift profiles shown in Fig. 10(a), it is evident that the injection duration for 200 bar injection pressure is approximately 17 CAD (1.88 ms). The separation between EOI (317 CAD) and SOC (335 CAD) is approximately 18 CAD (2 ms). A distinct LTHR is present for all injection pressures at around 338 CAD. The LTHR is related to the SOI and the in-cylinder residence time of the pilot diesel fuel before SOC. Because SOI was kept constant at 300 CAD for the range of injection pressures, the magnitude of LTHR is slightly suppressed with increasing injection pressure, whereas the location of LTHR with respect to TDC remains constant. The magnitude of peak AHRR increases and the SOC shifts toward TDC [Fig. 10(b)] as the injection pressure is increased. As the SOC is shifted toward TDC, the diesel sprays have more time to mix with the surrounding methane-air mixture. Consequently, a more premixed combustion process occurs and this facilitates faster overall burn rates. Moreover, as the diesel is injected at higher pressures, enhanced entrainment and turbulent mixing because of high jet momentum ensure availability of more prepared diesel-methane-air mixture when the in-cylinder temperature and pressure are high enough to support autoignition. Simultaneous autoignition of higher amounts of prepared diesel-air mixture also resulted in high peak AHRR at high injection pressures.

Fig. 11 shows the SOC (i.e., CA5), combustion phasing (CA50), and combustion duration (CA10-90) over the range of injection pressures investigated. The CA50 is phased progressively closer to TDC as the injection pressure is increased from 200 to 1,300 bar while the CA10-90 decreases with increasing injection pressure. The combustion process is phased closer to TDC at higher injection pressures because of enhanced turbulent mixing of diesel with the surrounding methane-air mixture, which is caused by the greater jet momentum at higher injection pressures.

As shown in Fig. 12, MPRR decreases and ID increases with increasing injection pressure. These trends further support the reasons discussed earlier for CA50 and CA10-90 behavior. The increase in ID with increasing injection pressure leads to longer residence times for the diesel to mix with the methane-air mixture, thereby creating a *well-mixed* mixture at high injection pressures. Further, the probability of spray impingement on the cylinder walls is increased with increasing injection pressure, especially for the early SOI of 300 CAD for these experiments. These factors combined to delay the CA50 as injection pressure is increased, thereby decreasing the MPRR. The COV of IMEP for the rail pressure sweep remained nearly invariant between 2.1 and 2.5%; and therefore, COV of IMEP is not included in Fig. 12.

Fig. 13 shows the combustion efficiency and IFCE trends with injection pressures. Combustion efficiency increased slightly as the injection pressure is increased from 200 to 1,300 bar. Combustion at 1,300 bar is characterized by CA50 phased closer to TDC and

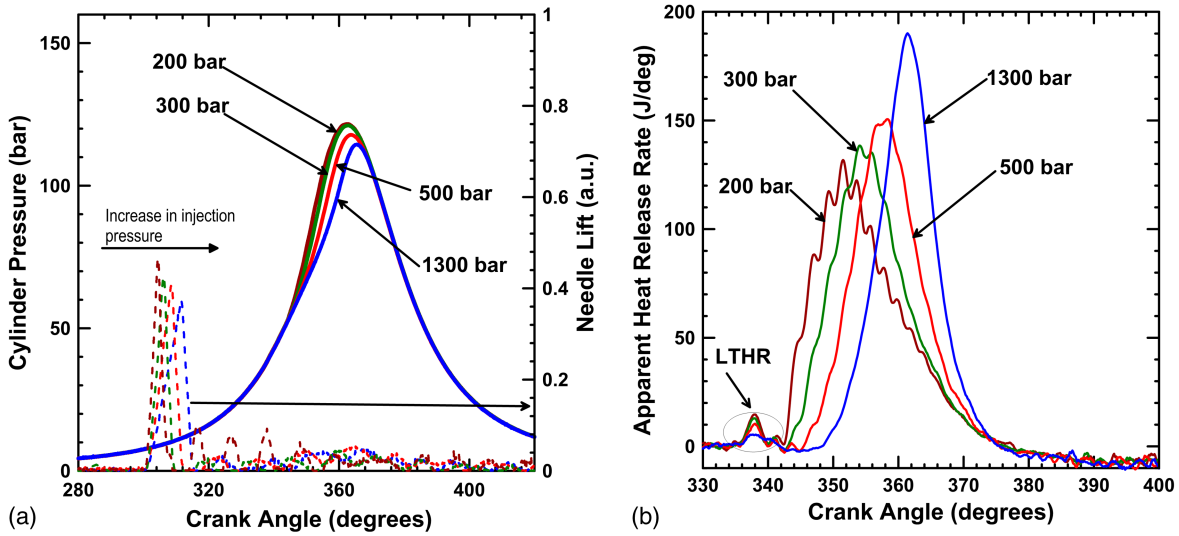

Fig. 10. (a) Cylinder pressure and needle lift profiles for various injection pressures at 5.1 bar IMEP, 80 PES, N = 1,500 rpm, Pin = 1.5 bar, 300 CAD SOI; (b) AHRR schedules for various injection pressures at 5.1 bar IMEP, 80 PES, N = 1,500 rpm, Pin = 1.5 bar, 300 CAD SOI

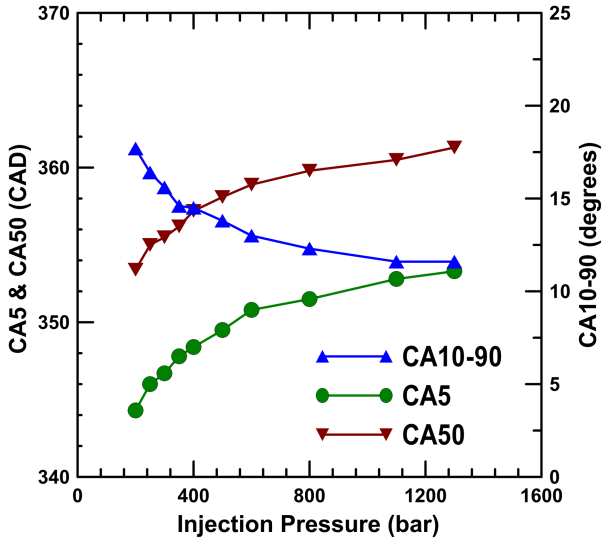

Fig. 11. CA5, CA50, and CA10-90 for various injection pressures at 5.1 bar IMEP, 80 PES, N = 1,500 rpm, Pin = 1.5 bar, 300 CAD SOI

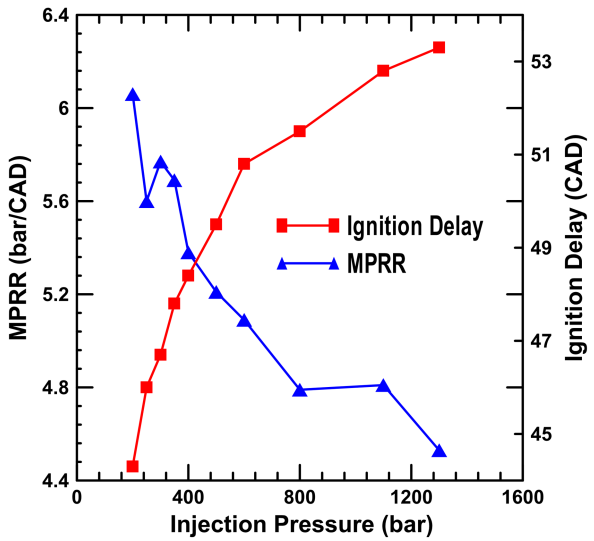

Fig. 12. MPRR and ignition delay for various injection pressures at 5.1 bar IMEP, 80 PES, N = 1,500 rpm, Pin = 1.5 bar, 300 CAD SOI

shorter combustion durations; therefore, the IFCE and combustion efficiency are slightly higher.

Fig. 14 represents ISNOx and smoke emissions with injection pressure variations. As injection pressure is increased from 200 to 1,300 bar, ISNOx emissions decrease significantly from 2.3 g/kW · h to near-zero levels (less than 0.1 g/kW · h), whereas the smoke emissions levels are constant (less than 0.1 FSN). The high value of NOx at 200 bar injection pressure is likely because of the fact that the injection duration is longer to keep the same diesel-injected quantity as evident from the needle lift profile shown in Fig. 10(a). As a result, the combustion is probably more stratified and characterized by high local temperatures that favor thermal NO formation. In contrast, as injection pressure increases, the injection duration decreases, the separation between EOI and SOC increases, and most importantly, diesel fuel is mixed more completely with the surrounding methane-air mixture before the onset of combustion. Fig. 10(a) shows that with increasing injection pressure, the cylinder pressure profiles are shifted away from TDC. As a result, the ignition delays are longer and combustion is increasingly homogeneous and occurs at low local temperatures, thus alleviating thermal NO formation. From Fig. 14, it is evident that the *optimum* injection pressure vis-à-vis ISNOx emissions is 500 bar (*only* under the present conditions), beyond which there is very little change in the ISNOx levels. Engine-out smoke emissions are low throughout the injection pressure sweep because of the high PES of methane (80%) and the overall lean combustion process in the methane-air mixture, regardless of injection pressure.

Fig. 15 shows the ISHC and ISCO emissions trends with injection pressures. The ISHC emissions steadily decrease from

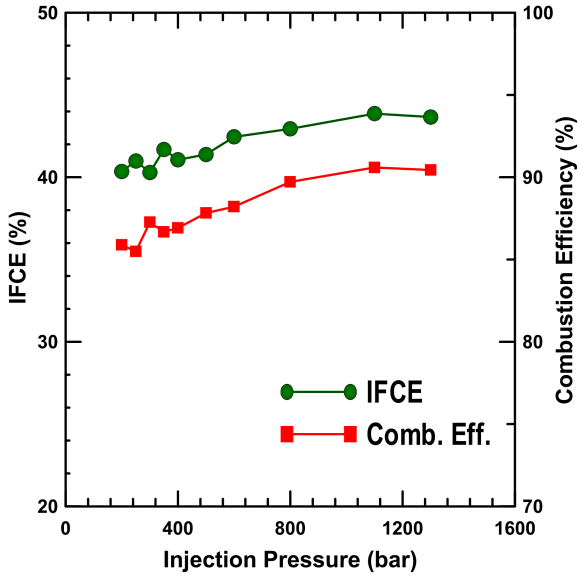

Fig. 13. Combustion and indicated fuel conversion efficiencies for various injection pressures at 5.1 bar IMEP, 80 PES, $N = 1{,}500$ rpm, Pin = 1.5 bar, 300 CAD SOI

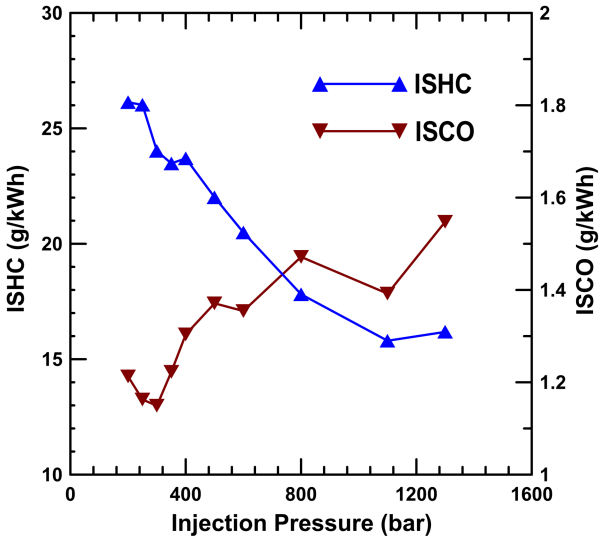

Fig. 15. ISHC and ISCO emissions for various injection pressures at 5.1 bar IMEP, 80 PES, $N = 1{,}500$ rpm, Pin = 1.5 bar, 300 CAD SOI

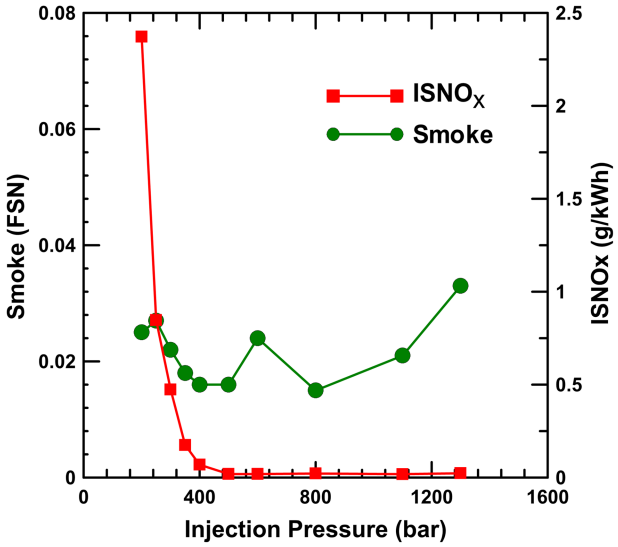

Fig. 14. ISNOx and smoke emissions for various injection pressures at 5.1 bar IMEP, 80 PES, $N = 1{,}500$ rpm, Pin = 1.5 bar, 300 CAD SOI

approximately 26 g/kW · h at 200 bar to approximately 16 g/kW · h at 1,300 bar injection pressure. This trend also corroborates the higher combustion efficiencies at higher injection pressures. Higher injection pressures lead to better fuel-air mixing and a more homogeneous combustion process, which also facilitates better mixing of high-temperature diesel combustion zones with leaner, low-temperature methane combustion zones, and consequently, better HC oxidation. In contrast, only a slight increase in ISCO emissions is observed with increasing injection pressure. At higher injection pressures, better fuel-air mixing can cause mixture *overleaning* that leads to lower bulk gas temperatures, which inhibit the CO → CO_2 conversion. Combined with better HC oxidation and potential mixture overleaning, the shorter CA10-90 durations at higher injection pressure reduce the time available for CO oxidization as postcombustion gases cool, thereby increasing the CO emissions.

Intake Boost Pressure Effects

The effect of intake boost pressure variations (from 1.1 to 1.8 bar) were studied at 5.1 bar IMEP, 1,500 rpm, 80 PES, 300 CAD SOI, and an injection pressure of 500 bar.

Fig. 16 shows cylinder pressure and AHRR profiles for intake boost pressures ranging from 1.1 to 1.8 bar. As the intake boost pressure is increased, peak cylinder pressure is also increased as expected because of the greater charge mass trapped within the cylinder. Also, the SOC and the location of peak pressure occur earlier with increasing boost pressure. However, the AHRR profiles exhibit a different trend. Peak AHRR decreases and the location of peak AHRR advances with increasing intake boost pressure. As intake boost pressure increases, the in-cylinder pressures and temperatures both before and during combustion are higher; consequently, combustion occurs earlier. In addition, the advancement of SOC with increasing boost pressure can be attributed to the increase in the magnitude of LTHR and a slight advancement of the LTHR profile, which can lead to higher precombustion temperatures and faster preignition reactions. Another related aspect of these intake boost pressure experiments is that the overall equivalence ratio is also allowed to vary with boost pressure (because the engine load is fixed at 5.1 bar IMEP); the equivalence calculated from measured fuel and air mass flow rates decreased from 0.36 at 1.1 to 0.26 at 1.8 bar boost pressure. Clearly, the temporal phasing of the AHRR curves is also affected by the overall equivalence ratios.

Fig. 17 presents MPRR and ID trends, whereas Fig. 18 shows trends for CA5, CA50, and CA10-90 for different intake boost pressures. Whereas MPRR shows only a slight increase with increasing boost pressure, ID decreases from 52 CAD at 1.1 bar boost to approximately 45 CAD at 1.8 bar boost. A decrease in intake boost pressure reduces in-cylinder pressures and temperatures, thus increasing the ID period. In addition, the CA50 is also phased closer to TDC as the boost pressure is reduced. Finally, because the overall equivalence ratio also increases as boost pressure is

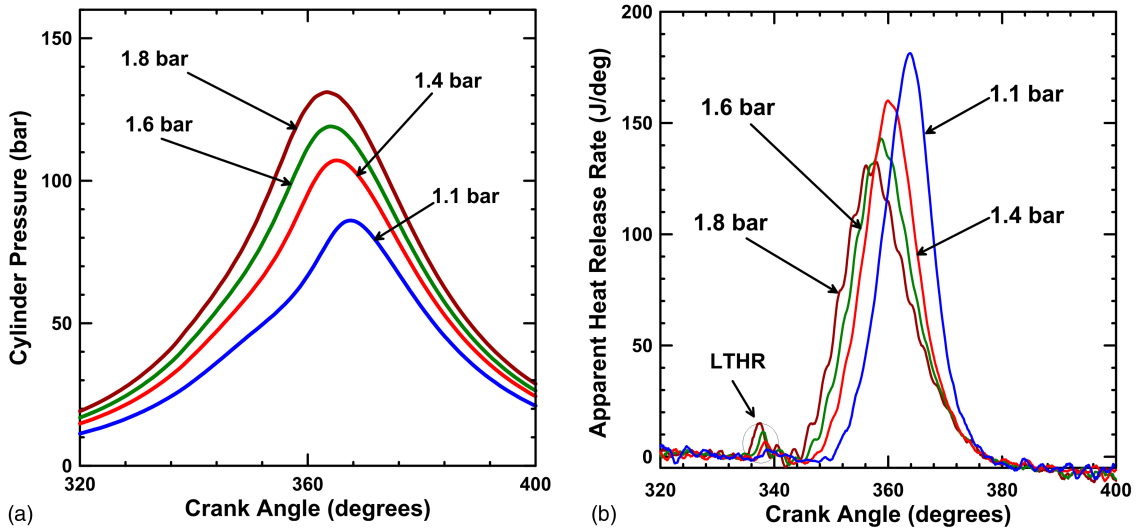

Fig. 16. (a) Cylinder pressure schedules for various intake boost pressures at 5.1 bar IMEP, 80 PES, $N = 1{,}500$ rpm, injection pressure = 500 bar, 300 CAD SOI; (b) AHRR schedules for various intake boost pressures at 5.1 bar IMEP, 80 PES, $N = 1{,}500$ rpm, injection pressure = 500 bar, 300 CAD SOI

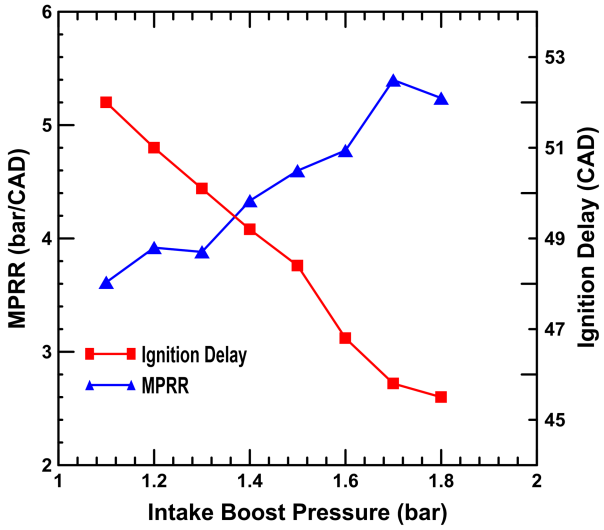

Fig. 17. MPRR and ignition delay for various injection pressures at 5.1 bar IMEP, 80 PES, $N = 1{,}500$ rpm, injection pressure = 500 bar, 300 CAD SOI

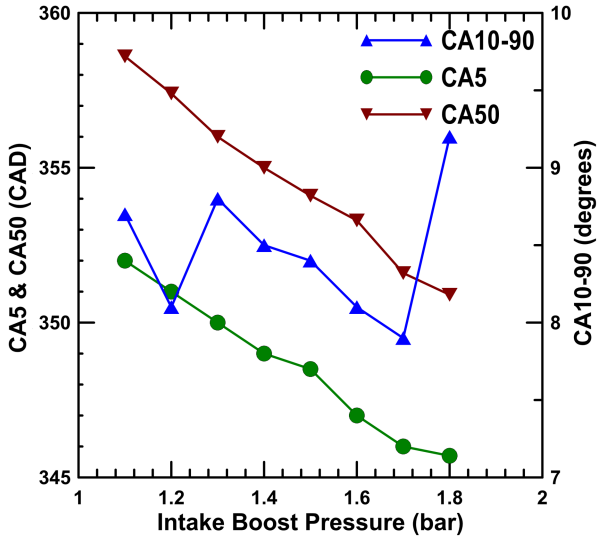

Fig. 18. CA5, CA50, and CA10-90 for various intake boost pressures at 5.1 bar IMEP, 80 PES, $N = 1{,}500$ rpm, injection pressure = 500 bar, 300 CAD SOI

decreased, the combustion process occurs more rapidly, resulting in higher peak AHRR and slightly higher MPRR. However, the CA10-90 remains virtually unaffected by boost pressure. Additionally, for reference, the COV of IMEP (not shown in Fig. 17) increased slightly from 1.7% at 1.1 bar to 2.5% at 1.8 bar of boost pressure.

The effect of intake boost pressure on IFCE, combustion efficiency, ISNOx, smoke, ISHC, and ISCO emissions are shown in Figs. 19–21. With the increasing of intake boost pressure, the IFCE decreases from 45% at 1.1 bar to 42% at 1.8 bar, whereas the combustion efficiency decreases from 92 to 84%. This is because of the fact that both CA5 and CA50 are phased earlier, i.e., farther away from TDC for higher boost pressures as shown in Fig. 18. For example, at the lowest boost pressure of 1.1 bar, the CA50 occurs at approximately 359 CAD but is phased near 351 CAD at 1.8 bar boost pressure. Because CA50 is phased closer to TDC, the IFCE is higher at lower boost pressures. In addition, because of the higher overall equivalence ratios at the lower boost pressures, the combustion efficiency is also higher.

Fig. 20 shows that faster AHRR and higher local temperatures lead to an increase in ISNOx emissions for boost pressures lower than 1.3 bar. However, the smoke emissions remain very low (i.e., <0.1 FSN) and fairly invariant with intake boost pressure. From Fig. 21, it is evident that as intake boost pressure is increased, both ISHC and ISCO increase. These trends can be explained with the AHRR profiles shown in Fig. 16(b). In most combustion processes (Glassman and Yetter 2008), fuel is initially oxidized into CO, and subsequently, CO oxidation to CO_2 occurs in the presence of hydroxyl radicals (OH) and oxygen and in sufficiently high-temperature regions that promote such oxidation. From the AHRR

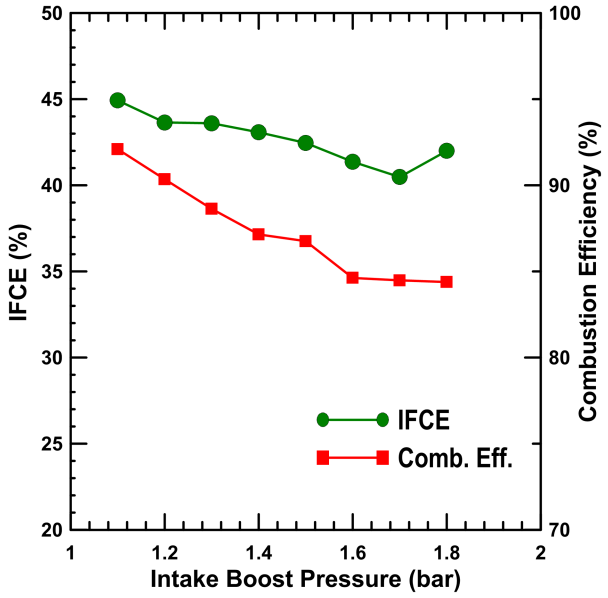

Fig. 19. Combustion and indicated fuel conversion efficiencies for various intake boost pressures at 5.1 bar IMEP, 80 PES, $N = 1{,}500$ rpm, injection pressure = 500 bar, 300 CAD SOI

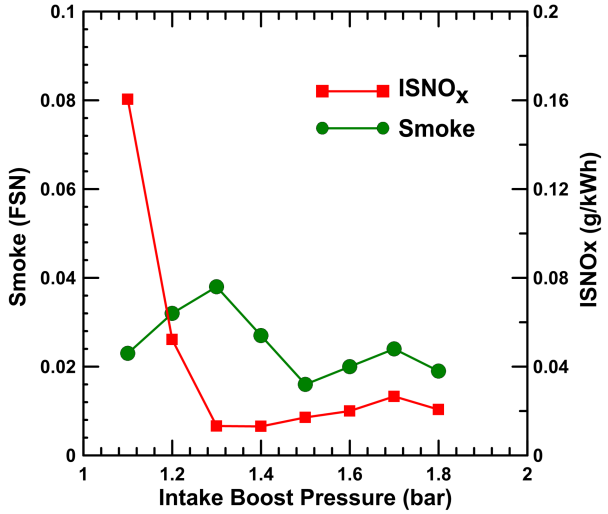

Fig. 20. ISNOx and smoke emissions for various intake boost pressures at 5.1 bar IMEP, 80 PES, $N = 1{,}500$ rpm, injection pressure = 500 bar, 300 CAD SOI

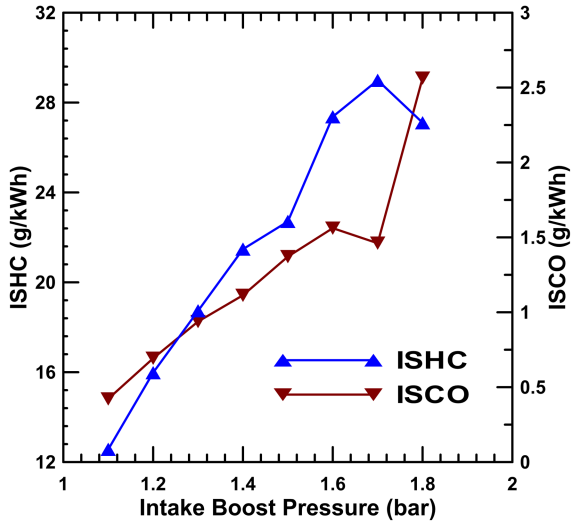

Fig. 21. ISHC and ISCO emissions for various intake boost pressures at 5.1 bar IMEP, 80 PES, $N = 1{,}500$ rpm, injection pressure = 500 bar, 300 CAD SOI

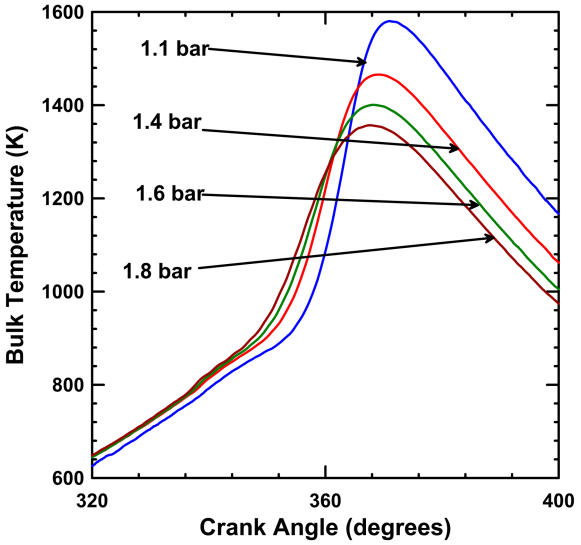

Fig. 22. Bulk gas temperature schedules for various intake boost pressures at 5.1 bar IMEP, 80 PES, $N = 1{,}500$ rpm, injection pressure = 500 bar, 300 CAD SOI

profiles, peak AHRR is highest for the lowest intake boost pressure of 1.1 bar and the bulk gas temperatures are also the highest for this condition as shown in Fig. 22, thereby assisting in better oxidation of CO to CO_2. In addition, the higher equivalence ratios at lower boost pressures will also aid in CO oxidation. The ISHC trends are also similar because they also increase when bulk gas temperatures are reduced. Also, as unburned fuel trapped in the crevices are one of the main sources of HC emissions, it is possible that higher intake boost pressures (leading to higher in-cylinder pressures) will result in trapping more unburned methane in the crevices. A significant fraction of the unburned methane trapped in crevices may not burn before exhaust valve opens because of incomplete mixing with hot postcombustion gases and unfavorable temperature-time histories.

Conclusions

Diesel-ignited methane dual-fuel combustion experiments were performed in a single-cylinder research engine (SCRE) at a constant speed of 1,500 rpm, a constant load of 5.1 bar net IMEP, and a constant methane percent energy substitution (PES) of 80%. Diesel injection timing (SOI: 250–350 CAD), diesel injection pressure (200–1,300 bar), and intake boost pressure (1.1–1.8 bar) were varied to assess their impact on combustion heat release (AHRR), indicated fuel conversion efficiency (IFCE) and combustion efficiency, and engine-out ISNOx, ISHC, ISCO, and smoke emissions. The experimental results obtained in this study lead to the following conclusions:

- Advancing SOI from 330 CAD to 300 CAD reduced ISNOx from 11.9 g/kW · h to less than 0.02 g/kW · h; further advancement of SOI did not yield significant ISNOx reduction.

Smoke emissions were less than 0.1 FSN at all SOIs. ISHC and ISCO emissions were very high for very late and at very early SOIs. The IFCE increased from 29.4 to 40.5% as SOI was advanced from 350 CAD to 300 CAD because of better combustion efficiencies, favorable combustion phasing, and shorter combustion durations. Combustion efficiency deteriorated at very late (350–340 CAD) and very advanced SOIs (270 CAD–250 CAD) because of substantially higher ISHC and ISCO emissions. Within the 250–350 CAD SOI range, the maximum pressure rise rate (MPRR) peaked at 10.4 bar/CAD for 330 CAD SOI but was reduced significantly (<4 bar/CAD) for SOIs earlier than 300 CAD. In contrast, ignition delay increased steadily with SOI advancement.

- An injection pressure sweep from 200 to 1,300 bar at 300 CAD SOI and 80 PES showed that very low injection pressures apparently led to more heterogeneous combustion and higher ISNOx, ISCO, and ISHC emissions whereas smoke remained unaffected. The intermediate injection pressure of 500 bar appeared to be optimal vis-à-vis performance and emissions under these conditions. Combustion efficiency and IFCE were unaffected but ignition delay increased and MPRR was reduced with increasing injection pressure.
- An intake boost pressure sweep from 1.1 to 1.8 bar at 500 bar injection pressure, 300 CAD SOI, and 80 PES showed that ISNOx and smoke remained fairly low at all conditions (ISNOx < 0.15 g/kW · h; smoke < 0.1 FSN) and unaffected by boost pressure. However, increasing intake boost pressure increased both ISHC and ISCO emissions. Whereas IFCE remained unaffected, combustion efficiency decreased from 92% at 1.1 bar intake boost pressure to approximately 84% at 1.8 bar.

Acknowledgments

The authors gratefully acknowledge the financial support from the Sustainable Energy Research Center (US DOE Award # DE-FG36-06GO86025) and the facilities support from the Center for Advanced Vehicular Systems at Mississippi State University.

References

Abd Alla, G. H., Soliman, H. A., Badr, O. A., and Abd Rabbo, M. F. (2000). "Effect of pilot fuel quantity on the performance of a dual fuel engine." *Energy Convers. Manage.*, 41(6), 559–572.

Abd Alla, G. H., Soliman, H. A., Badr, O. A., and Abd Rabbo, M. F. (2002). "Effect of injection timing on the performance of a dual fuel engine." *Energy Convers. Manage.*, 43(2), 269–277.

Agarwal, A. K. (2007). "Biofuels (alcohols and biodiesel) applications as fuels for internal combustion engines." *Prog. Energy Combust. Sci.*, 33(3), 233–271.

Badr, O., Karim, G. A., and Liu, B. (1999). "An examination of the flame spread limits in a dual fuel engine." *Appl. Therm. Eng.*, 19(10), 1071–1080.

Beck, N. J., Barkhimer, R. L., Johnson, W. P., Wong, H. C., and Gebert, K. (1997). "Evolution of heavy duty natural gas engines—Stoichiometric, carbureted and spark ignited to lean burn, fuel injected and micro-pilot." *SAE Technical Paper 972665*.

Bedoya, I. D., Arrieta, A. A., and Cadavid, F. J. (2009). "Effects of mixing system and pilot fuel quality on diesel–biogas dual fuel engine performance." *Bioresour. Technol.*, 100(24), 6624–6629.

Brunt, M., Rai, H., and Emtage, A. (1998). "The calculation of heat release energy from engine cylinder pressure data." *SAE Technical Paper 981052*.

Carlucci, A. P., De Risi, A., Laforgia, D., and Naccarato, F. (2008). "Experimental investigation and combustion analysis of a direct injection dual-fuel diesel–natural gas engine." *Energy*, 33(2), 256–263.

Chen, Z., Yao, M., Zheng, Z., and Zhang, Q. (2009). "Experimental and numerical study of methanol/dimethyl ether dual-fuel compound combustion." *Energy Fuels*, 23(5), 2719–2730.

Contino, F., Dagaut, P., Dayma, G., Halter, F., Foucher, F., and Mounaïm-Rousselle, C. (2013). "Combustion and emissions characteristics of valeric biofuels in a compression ignition engine." *J. Energy Eng.*, 10.1061/(ASCE)EY.1943-7897.0000161, A4014013.

Daisho, Y., et al. (1995). "Combustion and exhaust emissions in a direct-injection diesel engine dual-fueled with natural gas." *SAE Technical Paper 950465*.

Debnath, B. K., Bora, B. J., Sahoo, N., and Saha, U. K. (2013). "Influence of emulsified palm biodiesel as pilot fuel in a biogas run dual fuel diesel engine." *J. Energy Eng.*, 10.1061/(ASCE)EY.1943-7897.0000163, A4014005.

Dec, J. E. (1997). "A conceptual model of DI diesel combustion based on laser-sheet imaging." *SAE Trans.*, 106(3), 1319–1348.

Dec, J. E. (2009). "Advanced compression-ignition engines—Understanding the in-cylinder processes." *Proc. Combust. Inst.*, 32(2), 2727–2742.

DieselNet. (2014). "US EPA heavy-duty engine emissions standards." ⟨http://www.dieselnet.com/standards/us/hd.php⟩ (Apr. 10, 2014).

Giakoumis, E. G., Rakopoulos, C. D., and Rakopoulos, D. C. (2013). "Assessment of NOx emissions during transient diesel engine operation with biodiesel blends." *J. Energy Eng.*, 10.1061/(ASCE)EY.1943-7897.0000136, A4014004.

Gibson, C. M., Polk, A. C., Shoemaker, N. T., Srinivasan, K. K., and Krishnan, S. R. (2011). "Comparison of propane and methane performance and emissions in a turbocharged direct injection dual fuel engine." *J. Eng. Gas Turbines Power*, 133(9), 092806.

Glassman, I., and Yetter, R. A. (2008). *Combustion*, 4th Ed., Academic Press, Waltham, MA.

Goldsworthy, L. (2012). "Combustion behavior of a heavy duty common rail marine diesel engine fumigated with propane." *Exp. Therm. Fluid Sci.*, 42, 93–106.

Hanson, R. M., Kokjohn, S. L., Splitter, D. A., and Reitz, R. D. (2010). "An experimental investigation of fuel reactivity controlled PCCI combustion in a heavy-duty engine." *SAE Int. J. Engines*, 3(1), 700–716.

Heywood, J. B. (1988). *Internal combustion engine fundamentals*, McGraw-Hill, New York.

Huestis, E., Erickson, P. A., and Musculus, M. P. (2007). "In-cylinder and exhaust soot in low-temperature combustion using a wide-range of EGR in a heavy-duty diesel engine." *SAE Technical Paper 2007-01-4017*.

Jindal, S., Nandwana, B. P., Rathore, N. S., and Vashistha, V. (2010). "Experimental investigation of the effect of compression ratio and injection pressure in a direct injection diesel engine running on Jatropha methyl ester." *Appl. Therm. Eng.*, 30(5), 442–448.

Karim, G. A. (2003). "Combustion in gas fueled compression ignition engines of the dual fuel type." *J. Eng. Gas Turbines Power*, 125(3), 827–836.

Kokjohn, S. L., Hanson, R. M., Splitter, D. A., and Reitz, R. D. (2011). "Fuel reactivity controlled compression ignition (RCCI): A pathway to controlled high-efficiency clean combustion." *Int. J. Engine Res.*, 12(3), 209–226.

Krishnan, S. R., et al. (2004). "Strategies for reduced NOx emissions in pilot-ignited natural gas engines." *J. Eng. Gas Turbines Power*, 126(3), 665–671.

Krishnan, S. R., Biruduganti, M., Mo, Y., Bell, S. R., and Midkiff, K. C. (2002). "Performance and heat release analysis of a pilot-ignited natural gas engine." *Int. J. Engine Res.*, 3(3), 171–184.

Kusaka, J., Okamoto, T., Daisho, Y., Kihara, R., and Saito, T. (2000). "Combustion and exhaust gas emission characteristics of a diesel engine dual-fueled with natural gas." *JSAE Rev.*, 21(4), 489–496.

Lee, D., Jho, Y., and Lee, C. S. (2013). "Effect of soybean and canola oil-based biodiesel blends on spray, combustion and emission characteristics in a diesel engine." *J. Energy Eng.*, 10.1061/(ASCE)EY.1943-7897.0000160, A4014012.

Liu, Z., and Karim, G. A. (1995). "The ignition delay period in dual fuel engines." *SAE Technical Paper 950466*.

McTaggart-Cowan, G., Bushe, W. K., Hill, P. G., and Munshi, S. R. (2004). "NOx reduction from a heavy-duty diesel engine with direct injection of natural gas and cooled exhaust gas recirculation." *Int. J. Engine Res.*, 5(2), 175–191.

McTaggart-Cowan, G. P., Reynolds, C. C. O., and Bushe, W. K. (2006). "Natural gas fuelling for heavy-duty on-road use: Current trends and future direction." *Int. J. Environ. Stud.*, 63(4), 421–440.

Musculus, M. P., Miles, P. C., and Pickett, L. M. (2013). "Conceptual models for partially premixed low-temperature diesel combustion." *Prog. Energy Combust. Sci.*, 39(2), 246–283.

Papagiannakis, R. G., and Hountalas, D. T. (2003). "Experimental investigation concerning the effect of natural gas percentage on performance and emissions of a DI dual fuel diesel engine." *Appl. Therm. Eng.*, 23(3), 353–365.

Papagiannakis, R. G., and Hountalas, D. T. (2004). "Combustion and exhaust emission characteristics of a dual fuel compression ignition engine operated with pilot diesel fuel and natural gas." *Energy Convers. Manage.*, 45(18), 2971–2987.

Papagiannakis, R. G., Hountalas, D. T., and Rakopoulos, C. D. (2007). "Theoretical study of the effects of pilot fuel quantity and its injection timing on the performance and emissions of a dual fuel diesel engine." *Energy Convers. Manage.*, 48(11), 2951–2961.

Papagiannakis, R. G., Rakopoulos, C. D., Hountalas, D. T., and Rakopoulos, D. C. (2010). "Emission characteristics of high speed, dual fuel, compression ignition engine operating in a wide range of natural gas/diesel fuel proportions." *Fuel*, 89(7), 1397–1406.

Polk, A. C., et al. (2014a). "Diesel-ignited propane dual fuel low temperature combustion in a heavy-duty diesel engine." *Trans. ASME J. Eng. Gas Turbines Power*, 136(9), 091509.

Polk, A. C., Carpenter, C. D., Srinivasan, K. K., and Krishnan, S. R. (2014b). "An investigation of diesel-ignited propane dual fuel combustion in a heavy-duty diesel engine." *Fuel*, 132, 135–148.

Polk, A. C., Gibson, C. M., Shoemaker, N. T., Srinivasan, K. K., and Krishnan, S. R. (2013). "Detailed characterization of diesel-ignited propane and methane dual-fuel combustion in a turbocharged direct-injection diesel engine." *Proc. IME Part D J. Automobile Eng.*, 227(9), 1255–1272.

Qi, Y., Srinivasan, K. K., Krishnan, S. R., Yang, H., and Midkiff, K. C. (2007). "Effect of hot exhaust gas recirculation on the performance and emissions of an advanced injection low pilot-ignited natural gas engine." *Int. J. Engine Res.*, 8(3), 289–303.

Rakopoulos, C. D., Rakopoulos, D. C., Giakoumis, E. G., and Dimaratos, A. M. (2010). "Investigation of the combustion of neat cottonseed oil or its neat bio-diesel in a HSDI diesel engine by experimental heat release and statistical analyses." *Fuel*, 89(12), 3814–3826.

Rakopoulos, D. C., Rakopoulos, C. D., Giakoumis, E. G., and Dimaratos, A. M. (2013). "Studying combustion and cyclic irregularity of diethyl ether as supplement fuel in diesel engine." *Fuel*, 109, 325–335.

Ryu, K. (2013a). "Effects of pilot injection timing on the combustion and emissions characteristics in a diesel engine using biodiesel–CNG dual fuel." *Appl. Energy*, 111, 721–730.

Ryu, K. (2013b). "Effects of pilot injection pressure on the combustion and emissions characteristics in a diesel engine using biodiesel–CNG dual fuel." *Energy Convers. Manage.*, 76, 506–516.

Sayin, C. (2010). "Engine performance and exhaust gas emissions of methanol and ethanol–diesel blends." *Fuel*, 89(11), 3410–3415.

Sayin, C., and Canakci, M. (2009). "Effects of injection timing on the engine performance and exhaust emissions of a dual-fuel diesel engine." *Energy Convers. Manage.*, 50(1), 203–213.

Sayin, C., Uslu, K., and Canakci, M. (2008). "Influence of injection timing on the exhaust emissions of a dual-fuel CI engine." *Renewable Energy*, 33(6), 1314–1323.

Selim, M. Y. (2004). "Sensitivity of dual fuel engine combustion and knocking limits to gaseous fuel composition." *Energy Convers. Manage.*, 45(3), 411–425.

Selim, M. Y. (2005). "Effect of engine parameters and gaseous fuel type on the cyclic variability of dual fuel engines." *Fuel*, 84(7), 961–971.

Shoemaker, N. T., Gibson, C. M., Polk, A. C., Krishnan, S. R., and Srinivasan, K. K. (2012). "Performance and emissions characteristics of bio-diesel (B100)-ignited methane and propane combustion in a four cylinder turbocharged compression ignition engine." *Trans. ASME J. Engi. Gas Turbines Power*, 134(8), 082803.

Singh, S., Krishnan, S. R., Srinivasan, K. K., Midkiff, K. C., and Bell, S. R. (2004). "Effect of pilot injection timing, pilot quantity and intake charge conditions on performance and emissions for an advanced low-pilot-ignited natural gas engine." *Int. J. Engine Res.*, 5(4), 329–348.

Splitter, D., Hanson, R., Kokjohn, S., and Reitz, R. (2011). "Reactivity controlled compression ignition (RCCI) heavy-duty engine operation at mid- and high-loads with conventional and alternative fuels." *SAE Technical Paper 2011-01-0363*.

Srinivasan, K. K., et al. (2006a). "The advanced injection low pilot ignited natural gas engine: A combustion analysis." *J. Eng. Gas Turbines Power*, 128(1), 213–218.

Srinivasan, K. K., Krishnan, S. R., and Midkiff, K. C. (2006b). "Improving low load combustion, stability, and emissions in pilot-ignited natural gas engines." *Proc. IME Part D J. Automobile Eng.*, 220(2), 229–239.

Srinivasan, K. K., Krishnan, S. R., Qi, Y., Midkiff, K. C., and Yang, H. (2007). "Analysis of diesel pilot-ignited natural gas low-temperature combustion with hot exhaust gas recirculation." *Combust. Sci. Technol.*, 179(9), 1737–1776.

Tira, H. S., et al. (2014). "Influence of fuel properties, hydrogen, and reformate additions on diesel-biogas dual-fueled engine." *J. Energy Eng.*, 10.1061/(ASCE)EY.1943-7897.0000173, A4014003.

Wong, H. C., Beck, N. J., and Chen, S. K. (2000). "The evolution of compression ignition natural gas engines for low emission vehicles." *Proc., 2000 Fall Technical Conf. of the ASME Internal Combustion Engine Division, Paper No. (2000-ICE-318)*, Peoria, IL.

Yao, M., Chen, Z., Zheng, Z., Zhang, B., and Xing, Y. (2006). "Study on the controlling strategies of homogeneous charge compression ignition combustion with fuel of dimethyl ether and methanol." *Fuel*, 85(14), 2046–2056.

Zheng, M., Reader, G. T., and Hawley, J. G. (2004). "Diesel engine exhaust gas recirculation—A review on advanced and novel concepts." *Energy Convers. Manage.*, 45(6), 883–900.